Gravity- and strain-induced electric fields outside metal surfaces

F. Rossi and G. I. Opat
School of Physics, The University of Melbourne, Parkville, Victoria, 3052, Australia
(Received 26 November 1991)

The gravity-induced electric field outside a metal object supported against gravity is predominantly due to its differential compression which arises in supporting its own weight. This Dessler-Michel-Rorschach-Trammell (DMRT) field, as it has come to be known, is expected to be proportional to the strain derivative of the work function of the surface. We report the results of an experiment designed to produce this effect with mechanically applied strain rather than with gravity. In essence, we have measured the strain-induced contact-potential variation between a metal surface of known strain gradient and an unstrained capacitive probe. We describe useful solutions to the problems faced in such an experiment, which were not adequately addressed by earlier workers. A knowledge of the DMRT field is of considerable importance to experiments designed to compare the gravitational acceleration of charged particles and antiparticles inside a metallic shield. Past experiments with electrons yielded results contrary to the then-expected DMRT field. We review and partially extend the theoretical background by drawing on later results based on the jellium model of metal surfaces. Our results for Cu and Au surfaces are consistent with jellium-based calculations which imply a DMRT field that is about an order of magnitude smaller and of opposite sign to the early estimates.

I. INTRODUCTION

Gravity induces an electric field outside a supported metal object by redistributing the electrons and nuclei. We report the results of an experiment to investigate one component of this electric field, which has become known as the DMRT field (Dessler, Michel, Rorschach, and Trammell[1]), which is expected to dominate the external gravity-induced electric field. Another much smaller electric field, which must act on each electron to support it against gravity, was first discussed by Schiff and Barnhill.[21] The origin of the DMRT field is in the differential compression of the metal as it supports its own weight. This strain gradient produces a vertical gradient in the work function of the metal's surface, which, in equilibrium, implies that there must be a similar electrostatic potential variation just outside the surface. Our experiment produces the same effect with mechanically applied strain rather than that due to gravity. We measure the contact-potential variation between a differentially strained metal surface and an unstrained capacitive sensing probe.

An understanding of the DMRT field is of considerable importance to other experiments seeking to measure the gravitational acceleration of charged elementary particles and antiparticles, which, in essence, test the weak equivalence principle. Such experiments (see also Ref. 2 for a review) have been performed on electrons (Witteborn and Fairbank,[3] henceforth referred to as WF), proposed for positrons,[4,5] and one is currently under development for antiprotons and H^- ions.[6,7]

The difficulties in such experiments are extreme as the particles are charged.[2] For electrons and antiprotons, a vertical electric field of only -5.6×10^{-11} and -1.02×10^{-7} V/m, respectively, balances gravity. Witteborn's[8] pioneering work at Stanford appeared to demonstrate that free electrons could be satisfactorily shielded from most extraneous electric fields by enclosing them in a vertical copper drift tube cooled to 4.2K in ultrahigh vacuum. However, this is at odds with calculations of the expected gravity-induced electric field in the drift tube, which should preclude any measurement of the force of gravity.[1] A motive for the present experiment was to clarify this matter. Unlike earlier attempts at such measurements, the known strain gradient distribution in our sample surface allows us to convincingly establish the presence of the external tangential electric field posited by DMRT.

In Sec. II we briefly review the results of the experiments on electrons as well as the theoretical background of the DMRT field. In Sec. III we extend this by drawing on more modern studies of metal surfaces. In Sec. IV, we examine strain-induced contact potentials produced by mechanically deforming a metal body rather than by gravity, briefly reviewing earlier work, which we believe did not adequately account for or even consider some spurious effects. We identify the sources of error, and outline our improved technique. A more detailed account of the apparatus and technique was given by Rossi,[9] and will be the subject of a future paper to be published elsewhere.[10] We present our results in Sec. V, and a summary in Sec. VI.

II. ELECTRIC FIELDS IN DRIFT TUBE EXPERIMENTS

A detailed account of the apparatus and techniques used by WF to measure the gravitational acceleration of free electrons inside, their drift tube was given by Witteborn and Fairbank[11] (see also Darling *et al.*,[2] and Rossi[9]). In essence, measurement of the time of flight of

bursts of electrons emitted upwards through the drift tube determines the ambient force on the electrons, ideally only gravity. WF found the net acceleration of electrons inside the drift tube to be $(0\pm0.09)g$. This null result, rather than a downward acceleration of g, was attributed to the presence of a gravity-induced electric field which exactly cancels the force of gravity on electrons.

The great challenge of the WF experiment was to eliminate all nongravitational forces acting on the electrons. However, unlike idealized shields, real electrostatic shields, such as the drift tube, are not electrostatic equipotentials due to contact-potential phenomena. In thermodynamic equilibrium, any two metal surfaces with different work functions have different electrostatic potentials. Equilibrium may be established by an electrical connection which allows the transfer of electrons. The *contact-potential difference*, $\mathcal{V}$, is given by the difference of the work functions, viz.,

$$\mathcal{V}\equiv\phi_{01}-\phi_{02}=\frac{1}{e}(W_2-W_1)\ , \tag{1}$$

where ϕ_{01} and ϕ_{02} are the electrostatic potentials just outside the surfaces, and W_1 and W_2 are their work functions.[12,13]

The work function may vary over a polycrystalline metal surface due to inequivalent crystal facets or due to a nonuniform contamination (the patch effect[2,8,14–17]). Gravity also changes the work function by differentially compressing the metal. The DMRT field (discussed below) simply has its origin in a continuous, vertical, gravitational-strain-induced contact-potential variation on the metal's surface.

Witteborn[8] argued that the random potential variations on the drift tube axis, due to patches on its surface, could be reduced to almost acceptable levels if an amorphous surface were used, where the patch size would be of the order of atomic dimensions. By electroforming the copper, he produced a polycrystalline surface with crystallites smaller than 1 μm. Subsequent extended exposure to air produced an oxide layer 20–50 Å thick,[18] including other chemisorbed species. Other oxidation data[19] suggest that a thicker oxide layer 100–200 Å forms in a few hours. The drift tube was baked at 100 °C *in situ*, which would have driven off adsorbed water vapor, leaving most of the contaminant layer. Much higher temperatures and ion bombardment are required to produce an atomically clean surface.[20] Although the underlying copper is polycrystalline, the relatively large thickness (compared to interatomic dimensions) and complex chemistry of the contaminant layer would make the surface nearly amorphous. Investigations by Darling[16] on similar surfaces seem to confirm that the crystallinity is masked.

Before WF, Schiff and Barnhill[21] had calculated the vertical gravity-induced electric field in the drift tube to be

$$\mathbf{E}_{\rm SB}=-(mg/e)\hat{\mathbf{z}}\ , \tag{2}$$

(henceforth referred to as the SB field), where m is the electron's gravitational mass, e is the magnitude of the electron's charge, g is the magnitude of the acceleration due to gravity, and $\hat{\mathbf{z}}$ is a unit vector in the upward direction. Such an electric field is necessary to equilibrate the force of gravity on conduction electrons within the drift tube walls. It should also *exactly cancel* the force of gravity on an electron on the axis. Thus the WF null result was perfectly consistent with the presence of the SB field, the *absence* of the patch effect, and a *normal* gravitational acceleration for free electrons.

Soon after WF, Dessler *et al.*[1] (DMRT) published their calculation of the gravity-induced electric field, finding in addition to the SB field an upward field due to a vertical gradient in the work function

$$\mathbf{E}_{\rm DMRT}=\frac{1}{e}\frac{\partial W}{\partial z}\hat{\mathbf{z}}$$

$$=\gamma(Mg/e)\hat{\mathbf{z}}\ , \tag{3}$$

where M is the atomic mass (of Cu in this case), and γ is a dimensionless constant, estimated to be of order 0.1. The variation of the work function arises from the nonuniform compression of the metal as the lower layers support the weight of those above. The resulting fractional change in volume or dilation, u, and number density of atoms, n, are given by

$$u=\frac{\rho g}{3K}(z-H)\ , \tag{4}$$

$$n\approx n_0(1-u)\ , \tag{5}$$

where ρ is the mass density, K is the bulk modulus of compression, H is the height of the drift tube, and n_0 is the number density before deformation. Thus γ is given by

$$\gamma=\frac{n_0}{3K}\frac{\partial W}{\partial u}\ , \tag{6}$$

where $\partial W/\partial u$ is the strain derivative of the work function.

Since $M/m\approx10^5$, the DMRT field should have overwhelmed gravity and the SB field. Herring[22] reconciled the two calculations, and it is now generally agreed (Schiff[23]) that the DMRT calculation is *essentially* correct. It would seem then that either the DMRT and patch fields were being simultaneously masked or shielded, or that something was amiss in the experiment. In the former case, the shielding effect must be very selective since the SB field and fields produced by running electric currents through the drift tube walls were not shielded.

Lockhart, Witteborn, and Fairbank[24] (henceforth referred to as LWF) originally claimed evidence for a temperature-dependent shielding effect operating at drift tube temperatures below about 4.5 K, however, these data have since been partially retracted.[25] Other experiments have failed to demonstrate any temperature-dependent shielding effect for patch fields.[16,26] These issues were investigated and discussed by Rossi[9] and Darling.[16]

In Eqs. (4) and (7) for the DMRT field, the most poorly known quantity is the strain derivative of the work func-

tion, $\partial W/\partial u$. Our experiments sought to better determine this quantity.

III. STRAIN DEPENDENCE OF WORK FUNCTIONS AND JELLIUM SURFACES

For surfaces with a nonuniform work function, an appropriate definition of the work function W is "the minimum energy required to remove an electron from the metal to rest just outside the surface".[12] "Just outside the surface" means beyond all significant interaction with the metal, including the image potential attraction, which implies distances of the order of 0.1–1 μm. The work function contains two contributions:

$$W=(-eD/\epsilon_0)-\mu$$
$$=\Delta\Phi-\mu\ , \tag{7}$$

where D is the areal density of the normal component of the surface dipole moment, ϵ_0 is the SI constant, and μ is the ordinary chemical potential in the bulk, containing the kinetic and exchange-correlation contributions to the electron's energy.[27] D depends on the state of the surface region of the metal, including the effects of the evanescent tunneling of electrons into the vacuum, and of the dipole moments of adsorbed foreign atoms. $\Delta\Phi$ is that part of the energy expended by an electron in passing through this dipole layer. The other term, μ, reflects the state of the interior of the metal.

In Eq. (7) for γ, the variation of W with height was assumed to be only due to the change in density, given by the dilation u. For a crystalline solid, this is expected to be true to first order,[28] however, higher-order terms are expected from deformation without a change in density, i.e., shear strain, particularly for the surface component D. For a polycrystalline solid, these corrections may average out over length scales much larger than the crystallites. For the drift tube, with a nearly amorphous contaminant surface, we would expect only the change in density to be significant, validating the use of Eq. (7).

As a first step, we consider a naive model of the work function, which neglects the change in D and takes μ as the Fermi kinetic energy for free electrons, ε_F, inside a fixed potential well, viz., $\mu\approx\varepsilon_F-\text{const}$. It is then straightforward to show that $\gamma=(2n_0/9K)\varepsilon_F=0.15$ for copper. This would make the DMRT field $+1.0$ μV/m (upwards), or about 18 000 times larger and oppositely directed to the SB field (-5.6×10^{-11} V/m).

DMRT considered a more accurate expression for μ and estimated the dependence of D on density, concluding that this would lower γ from the free electron estimate, but, barring accidental cancellation between D and μ, would leave an upward field 0.1–1.0 μV/m, still orders of magnitude larger than the SB field.

More modern studies of metal surfaces suggest a different picture. In the jellium model of metal surfaces, the lattice of ions is smeared out into a uniform positive background charge with an abrupt edge. A jellium metal is characterized by a single density parameter, the Wigner-Seitz radius r_s, i.e., the radius of a sphere that contains, on average, one conduction electron: $(4\pi/3)r_s^3=1/n_e$, where n_e is the number density of conduction electrons in the bulk. Although this simplification may seem too drastic and unrelastic, Lang and Kohn[29–31] have applied density functional theory to this model, with a local density approximation, with remarkable success for simple metals.

For the transition and noble metals, jellium is not as successful, e.g., the calculated work function for jellium copper is about 19% lower than that observed for polycrystalline samples. More sophisticated lattice models,[32] which include the effects of d-shell electrons,[33] reduce this discrepancy, but represent only single numerical results for W for specific crystal planes. Unfortunately, they do not yield much insight regarding the strain or density dependence of the work function. At present, jellium calculations, over a wide range of the density parameter r_s (Fig. 1), appear to be the only useful theoretical guide we have. Since $\partial W/\partial u=(r_s/3)\partial W/\partial r_s$, jellium finds a natural application in predicting the DMRT field.

In the case of the drift tube, we note that the relevant surface is that of the contaminant layer, so that it is not clear that any tractable theoretical model can be expected to yield accurate results. However, it seems plausible that such a nearly amorphous surface could be reasonably well described by a jellium of some density, though not necessarily the same density as the underlying copper.

It was not appreciated in early analyses of the DMRT field that there are, in fact, physical reasons for a large degree of cancellation between D and μ, which are borne out empirically and by jellium calculations. Heine and Hodges[34] have shown that μ and D are highly correlated for most of the nontransition-series metals. They suggest that this is due to a kind of feedback mechanism. If μ increases, raising the internal electron levels toward the

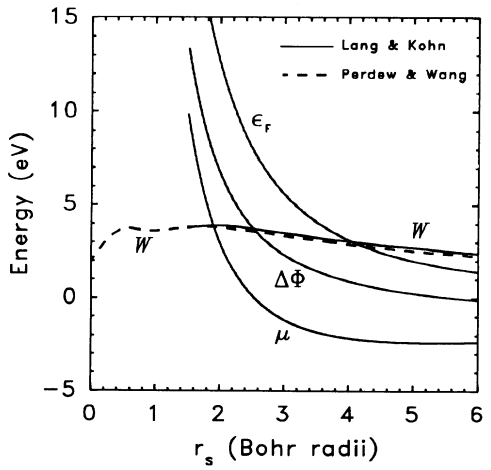

FIG. 1. Jellium work function and components vs density. $W=\Delta\Phi-\mu$, $\Delta\Phi=-eD/\epsilon_0$, and ε_F is the Fermi kinetic energy of a uniform electron gas. Increasing r_s means decreasing conduction electron density. $a_0=0.53$Å is the Bohr radius. From the results of Lang and Kohn (Ref. 27), Lang (Ref. 37) and Perdew and Wang (Ref. 38).

TABLE I. Strain derivative of jellium work function. For the normal range of densities encountered in metals. $a_0=0.53$ Å is the Bohr radius. $u>0$ corresponds to tension. The values given are the averages of those calculated from the results of Lang and Kohn (Ref. 27) and Perdew and Wang (Ref. 38) for W versus r_s.

	r_s (a_0)	$\partial W/\partial u$ (eV/unit strain)
	1.25	0.17
	1.76	0
	2	−0.09
(Cu)	2.67	−0.39
(Au)	3.01	−0.45
	4	−0.53
	5	−0.55
	6	−0.55

$-0.6<\partial W/\partial u<0.2$ eV/unit strain, $r_s>a_0$

vacuum, the electrons tunnel further out, making D more negative. Thus $\Delta\Phi=-eD/\epsilon_0$ increases and compensates for μ, maintaining $W=\Delta\Phi-\mu$ roughly constant.

The compilation by Michaelson[35] shows that the measured work functions of virtually all the transition metals cluster in a 1-eV-wide band centered on 4.5 eV, while μ varies by over 6 eV (Moruzzi, Janak, and Williams[36]). This behavior is clearly evident in Fig. 1, showing jellium calculations for W and its components as a function of density. While μ varies considerably, $\Delta\Phi$ almost mirrors it, leaving W only weakly dependent on density. For comparison, the density dependence of the Fermi kinetic energy, ϵ_F is also shown.

Table I shows $\partial W/\partial u$ as a function of r_s, as estimated from calculations for jellium.[27,37,38] A useful prediction is that $-0.6<\partial W/\partial u<0.2$ eV/unit strain over the entire density range encountered in metals under normal conditions ($r_s>1.3a_0$). We note that W has a broad maximum at $r_s\approx 1.8a_0$ ($a_0=0.53$ Å is the Bohr radius) in Fig. 1. If the surface of the WF drift tube behaved like a jellium with this density, it would have no DMRT field, since $\partial W/\partial u=0$. This may have some bearing on the WF null result. However, this still appears to require a remarkable coincidence, and moreover, that this condition is stable to changes in surface contamination.[9]

Table II summarizes these calculations of the DMRT field for pure copper ($r_s=2.67a_0$). We note that inclusion of the surface dipole layer lowers this field by almost an order of magnitude from the naive estimate based solely on ϵ_F. The dipole layer is clearly *not negligible* since it changes the sign of DMRT field from the original estimate.

This still leaves the DMRT field about 1500 times larger than the SB field and so should dominate over the force of gravity in drift tube experiments with electrons. For antiprotons it would be slightly smaller. However, we cannot realistically expect any theoretical model to accurately predict the DMRT field for impure surfaces with complex chemistries such as the drift tube's. The determination of $\partial W/\partial u$ for *real contaminated* surfaces was the aim of the experiments which we report in the remainder of this paper.

IV. STRAIN-INDUCED CONTACT-POTENTIAL TECHNIQUE

A. The DMRT field and contact potentials

As we have already noted, the electrostatic potential variation associated with the DMRT field may be considered simply as a continuous gravity-induced contact-potential variation along the surface. If $\phi_0(z)$ is the electrostatic potential just outside the surface at a height z, and $\phi_0(H)$ its value at the unstrained top, $z=H$, then [cf. Eq. (1)] the height-dependent contact potential $\mathcal{V}_g(z)$ is given by

$$\mathcal{V}_g\equiv\phi_0(H)-\phi_0(z)=\frac{1}{e}[W(z)-W(H)]\,, \tag{8}$$

where $W(z)$ and $W(H)$ are the corresponding values of the work function. The DMRT field is then given by [cf. Eq. (4)]

TABLE II. Theoretical estimates of the DMRT field for copper. ($r_s=2.67a_0$.) $a_0=0.53$ Å is the Bohr radius. A positive value of the field indicates that it is directed upwards. The last column compares the force produced by the DMRT field to that of gravity for particles used in drift tube experiments.

Theory	$\partial W/\partial u$ (eV/unit strain)	DMRT field (μV/m)	Ratio of electrical to gravitational force
ϵ_F only	4.7	1	18 000 for e^- and e^+ 10 for p and $\bar{p}$
DMRT	0.5–5	0.1–1	1800–18 000 1–10
Jellium	−0.39	−0.083	1500 0.8

$$\mathbf{E}_{\mathrm{DMRT}}=\frac{1}{e}\frac{\partial W}{\partial u}\frac{du}{dz}\hat{\mathbf{z}}$$
$$=\frac{d\mathcal{V}_g(z)}{dz}\hat{\mathbf{z}}\ , \tag{9}$$

where $\partial W/\partial u$ is the local strain derivative of the work function, and $u(z)$ is the gravity-induced volume dilation.

Contact potentials are normally measured by forming a closely spaced parallel-plate capacitor from the two electrically connected metal surfaces under study.[39,40] Often, one plate forms the sample surface, while the other reference plate (or probe) is vibrated, thereby modulating the spacing and the capacitance, and forcing an ac current to flow in a circuit such as in Fig. 2. While the contact potential $\mathcal{V}$ may be inferred from a measurement of this current, a more elegant and accurate technique is to insert a variable voltage source V_B (referred to as the bias voltage or the bucking voltage) in series with the capacitor, adjusting it until the current is nulled. Then, ideally, the electrostatic potential between the capacitor plates is nulled, whence, $V_B=-\mathcal{V}$. Thus measurement of V_B determines the contact potential with the advantage that the value of the capacitance need not be accurately known, although to increase the sensitivity it is made as large as is possible.

Perhaps the most direct way of sensing the DMRT field outside a tall metallic object supported against gravity would be with a small vibrating capacitive probe scanned up and down the length of the object. The contact potential between the probe, which forms the reference surface, and the small region on the object's surface directly opposite the probe, which forms the sample surface, would show a linear variation with height, equal to $\mathcal{V}_g$ in Eq. (9). However, this is fraught with error since on any real surface, the work function may vary by a significant fraction of an eV over its length due to the patch effect, whereas the gravitational variation is expected to be less than 1 μeV for a meter high object.

Presumably, it does not matter whether gravity or some other external force produces the local strain since Eqs. (4) and (7) give the DMRT field directly in terms of the local strain derivative of the work function. Instead of scanning a capacitive probe over a meter or so of surface, the position could be fixed and the local strain altered at will by externally applied forces. Then the change in contact potential,

$$\delta\mathcal{V}=\mathcal{V}_U=\frac{1}{e}\frac{\partial W}{\partial u}u\ , \tag{10}$$

for a known applied dilation u gives $\partial W/\partial u$ and hence the expected DMRT field at that point. This type of experiment is much more controllable, enabling large strains to be used, thereby increasing the size of the measurable effect.

We note that for comparisons with theory, it is essential to be clear on the sign of the work-function change implied by the measured strain-induced contact potential. We have found the reported results of some earlier experiments to be ambiguous in this respect. The convention we adhere to defines the contact potential as the difference between the electrostatic potential of the probe and that of the strained sample:

$$\mathcal{V}\equiv(\phi_{\mathrm{probe}}-\phi_{\mathrm{sample}})=(1/e)(W_{\mathrm{sample}}-W_{\mathrm{probe}})\ , \tag{11}$$

so that $\delta\mathcal{V}$ has the same sign as the change in the work function of the sample, $\delta W_{\mathrm{sample}}$.

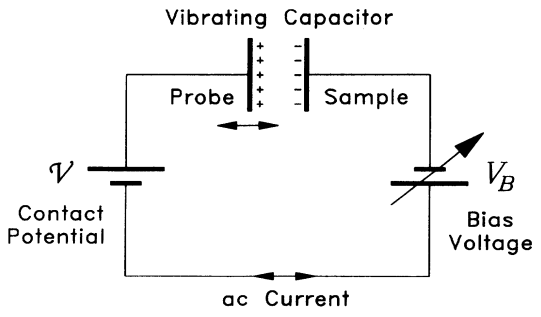

FIG. 2. Vibrating capacitor technique for measuring the contact potential $\mathcal{V}$, using a nulling bias voltage V_B.

B. Sources of error

Given the long history of contact-potential measurement technique and the simple arrangement we have outlined, it might seem that such an experiment is straightforward. In reality, it is very difficult due to a number of spurious effects associated with the application of strain to the sample. Considerable development beyond this simple idea is needed. We believe that several earlier experimenters (see Table III) who attempted measurements of strain-induced contact potentials did not adequately account for a number of spurious effects discussed below. We note that the jellium calculations imply that the strain-induced contact potential may be an order of magnitude smaller and of opposite sign to that originally estimated by DMRT. Most of the early results produced values well outside the bounds predicted by jellium (cf. Tables I and III); some[41–43] are much larger than even the naive estimate based on only ε_F; others have very large relative uncertainties attached.[44–46]

If the absence of the DMRT field implied by the drift tube experiments is a genuine effect, a crude strain-induced contact-potential measurement might miss this null due to the presence of unaccounted errors. Experiments should be able to do more than *just* see the expected strain-induced contact potential above commensurate noise and spurious effects. They should have enough reserve to clearly measure an anomalously low value. Given the lower predictions of jellium, which we believe are more realistic, the experimental requirements are much more stringent than those addressed by earlier workers. Space does not permit a complete discussion of our solutions to all these problems, however, a brief overview is necessary for the interpretation of data presented in subsequent sections. A comprehensive and critical discussion was given by Rossi,[9] and will be the subject of a separate paper planned to be published elsewhere.[10] Figure 3 summarizes the experimental arrangement, the

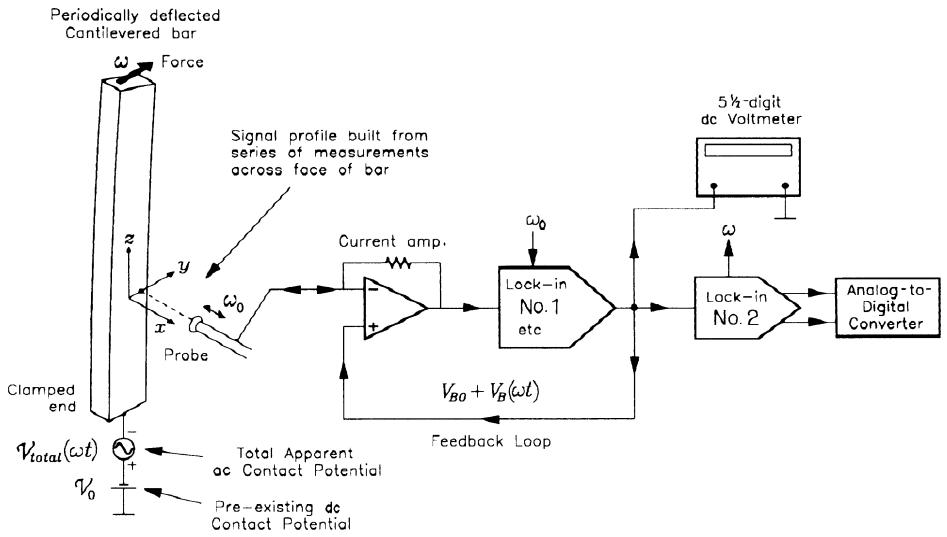

FIG. 3. Summary of experimental technique, showing cantilevered bar, synchronous feed-back loop, and additional instruments.

features of which will become clearer as the discussion proceeds.

1. *Periodic strain*

At the outset, it should be appreciated that contact potentials are very sensitive to surface conditions. Quite apart from effects concurrent with strain, they may drift by millivolts over short intervals while typical signal levels are expected to be of the order of microvolts. This problem alone demands that the applied strain be periodically modulated at some frequency ω, enabling the genuine variations to be extracted from drift (and random noise) by synchronous detection (lock-in) techniques. Then the *total apparent* strain-induced contact-potential signal $\mathcal{V}_{\text{total}}(\omega t)$, which includes a number of spurious signals discussed below, has in addition to an amplitude, a phase with respect to the applied strain. The genuine strain-induced contact potential $\mathcal{V}_U(\omega t)$ should be directly in phase with the strain [Eq. (11)], a feature

TABLE III. Strain derivative of the work function, and implied DMRT field. Summary of the results obtained by previous workers for various copper surfaces. Note that positive dilation, $u > 0$, corresponds to tension. The values quoted from Craig's paper are of opposite sign to the one given by him; it may be verified, by careful inspection of his measurement circuit, that his data do in fact imply the sign given here. A positive value indicates that the field is directed upwards.

Source of estimate	$\partial W/\partial u$ (eV/unit strain)	Implied DMRT field (μV/m)
	Experimental	
Beams (Ref. 53) (duraluminum)	>0	>0
Craig (Ref. 41)	$-(12-29)$	$-(2.6-6.4)$
French and Beams (Ref. 42)	4.7 ± 1.6	1.0 ± 0.4
	≈ -60	≈ -10
Brown *et al.* (Ref. 44)	-0.9 ± 2.3	-0.2 ± 0.5
	-0.14 ± 0.68	-0.03 ± 0.15
Guptill (Ref. 54)	2.7–3.0	0.60–0.67
Schumacher, Spicer, and Tiller (Ref. 43)	32	7
Leners, Kearney, and Dresser (Ref. 45)	-1.5 ± 9.8	-0.34 ± 2.2
	-6.9 ± 4.2	-1.5 ± 0.9
Enga (Ref. 55)	-2.8 ± 0.4	-0.61 ± 0.09
Mints, Melekhin, and Partenskii (Ref. 56)	>0	>0
Chow and Tiller (Ref. 46)	0 ± 2.4	0 ± 0.5
	Theoretical	
ε_F only	4.7	1
DMRT	0.5–5	0.1–1
Jellium	-0.39	-0.083

which may be used to distinguish it from spurious signals.

2. Strain gradient

To convincingly establish that the signals we measure are genuine, and not, for example, the result of some unrecognized coupling from the electrical straining system, we have introduced a known spatial profile for the strain on the sample surface. By scanning the probe over the sample, a profile of the signal may be built up, which should be the same as that of the strain. It is then clear that what has been measured is due to strain, and intrinsic to the sample.

Our apparatus produces a linear strain profile by using a cantilevered bar for the sample, which is periodically deflected in the y direction in Fig. 3. The probe is scanned across a strip on the y-z face of the bar, near its base. Solution of the elasticity equations[47] shows that the strain field corresponds to simple compression or extension along the z axis. On the strip sensed by the probe, the dilation is given by

$$u(y,\omega t)=u_0(2y/w)\sin(\omega t)\ , \tag{12}$$

where w is the width of the bar. Figure 4 shows this profile for actual experiment conditions (note that strain and dilation are dimensionless quantities). The maximum level of applied strain is about 1% of the elastic limit of the bar, or about 100 times larger than that present at the bottom of the WF drift tube. When deflected to the right as seen from the probe, the left half of the bar is in tension, while the right half is in compression. The spatial profiles of ω periodic quantities shown in subsequent sections correspond to this instant (Fig. 4–9).

In addition to its diagnostic use, this strain profile closely resembles the deformed state of an object supporting its own weight against gravity, such as a drift tube [Eq. (5)]. A measured strain-induced surface potential gradient then clearly establishes the presence of the DMRT field.

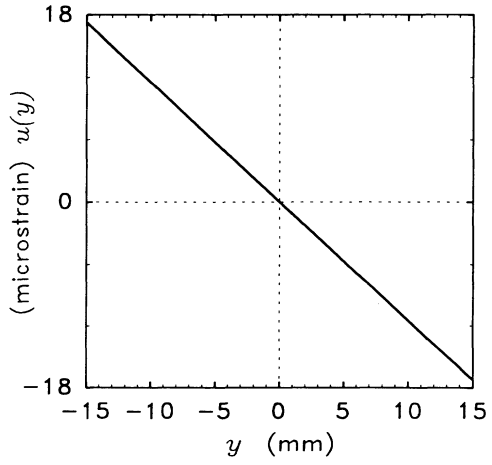

FIG. 4. Spatial profile of the periodic dilation $u(y,\omega t)$ for the conditions of the experiment, over the strip sensed by the probe, at the instant when the cantilevered bar is at its maximum positive y deflection. Note that dilation (or the fractional change in volume) is a dimensionless quantity, and that positive dilation corresponds to extension.

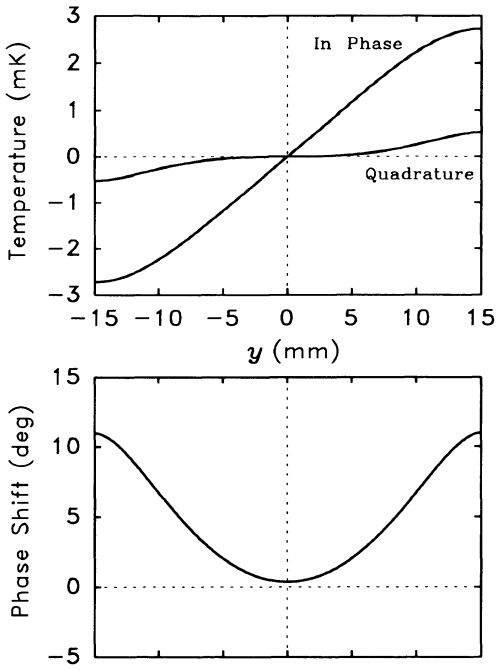

FIG. 5. Periodic strain-induced temperature variations over the region of the bar sensed by the probe, for $\omega/2\pi\approx 1$ Hz, calculated from the measured strain (Fig. 4). Upper graph: rectangular components of temperature phasor, $T(y)$. Lower graph: phase shift of temperature variations, $\theta_T(y)$, relative to dilation.

3. Spacing modulation error

When strained, the sample will expand or contact (even in directions normal to the applied stress, as described by Poisson's ratio), which means that the spacing between

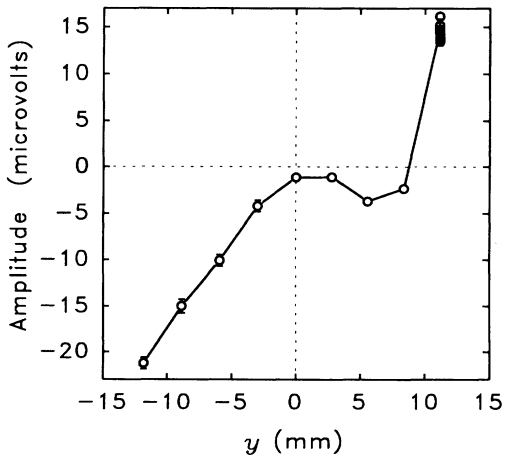

FIG. 6. Raw signal profile $\mathcal{V}_{\text{total}}(y)$ for Cu in presence of He gas at 1 Torr pressure, at room temperature.

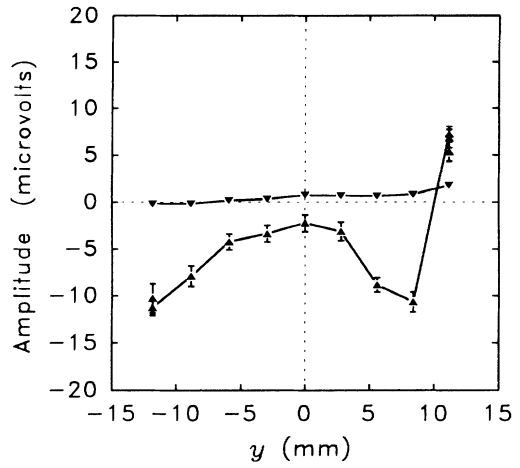

FIG. 7. Geometry error signal profiles, $\mathcal{V}_X(y)$ (down triangles) and $\mathcal{V}_Y(y)$ (up triangles), for Cu in presence of He gas at 1 Torr pressure, at room temperature.

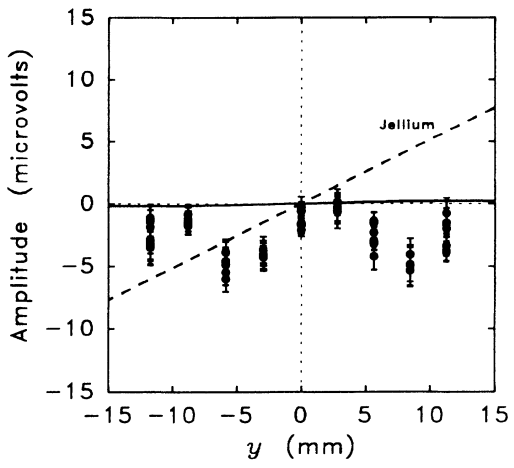

FIG. 9. Partially corrected signal profile $\mathcal{V}_{\text{total}}-\mathcal{V}_X-\mathcal{V}_Y$ for Au at 10^{-7} Torr pressure and room temperature. The solid line shows the fit of the combined signals $(\mathcal{V}_U+\mathcal{V}_T)$. The dashed line shows the expected profile for $\mathcal{V}_U(y)$, based on jellium calculations for pure Au ($r_s=3.01a_0$).

the sample and the capacitive probe will change periodically by some amount $a'(\omega t)$. Because the capacitor is charged with a preexisting (dc or static) contact potential $\mathcal{V}_0$, this change can produce a spurious signal, which we refer to as the spacing modulation error, $\mathcal{V}_X(\omega t)$. Ideally, a simple solution would be to null $\mathcal{V}_0$ with a bias voltage $\mathcal{V}_{B0}$ in the same way as one normally measures contact potentials with a vibrating probe. This nulling procedure should be served with a feedback loop arrangement which continuously tracks any drift in $\mathcal{V}_0$, so that the loop always maintains

$$V_{B0}=-G(0)\mathcal{V}_0\ , \tag{13}$$

where $G(0)\approx 1$ is the dc closed loop gain. If the probe vibration frequency ω_0 is much larger than the strain frequency, ω, an appropriately designed feedback loop may be made to track the strain-induced contact potential $\mathcal{V}_U(\omega t)$ as well. Then the loop's output (Fig. 3) contains, in addition to V_{B0}, a periodic component given by

$$V_B(\omega t)=-G(\omega)\mathcal{V}_{\text{total}}(\omega t)\ , \tag{14}$$

where $G(\omega)$ is the closed loop gain at ω. The most important measured quantities in this experiment are V_{B0} and $\mathcal{V}_B(\omega t)$, the latter yielding $\mathcal{V}_{\text{total}}(\omega t)$, and eventually, $\mathcal{V}_U(\omega t)$ after correction for other error sources discussed below.

However, the problem is more complicated than described above due to the generally observed spacing dependence of V_{B0},[48–50] and hence of the *apparent* contact potential $\mathcal{V}_0$. This arises from the patch effect, capacitive coupling to other surfaces, spurious ω_0 signals in the measurement circuit, dc offsets in the output stages of lock-in no. 1, and the intrinsic spacing dependence of $G(0)$. In relying on nulling $\mathcal{V}_0$, there is then no clear way of determining when the spacing modulation error is nulled. It may be shown[9,10] that in the presence of such effects $\mathcal{V}_X(\omega t)$ is proportional to the slope of $V_{B0}(x)$ as a function of capacitor spacing x, viz.,

$$\mathcal{V}_X(\omega t)=\frac{\partial V_{B0}}{\partial x}\frac{a'(\omega t)}{G(0)}\ . \tag{15}$$

if the observed $V_{B0}(x)$ curve has a maximum or minimum, then operation at that spacing eliminates the error signal. In cases where this does not naturally occur, one may be induced by deliberately injecting dc offsets or small ω_0 signals into the feedback loop.[9,10,50]

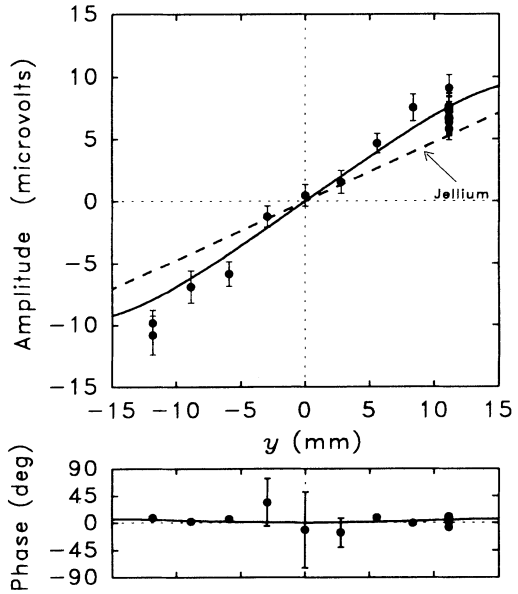

FIG. 8. Partially corrected signal profile $\mathcal{V}_{\text{total}}-\mathcal{V}_X-\mathcal{V}_Y$ for Cu in presence of He gas at 1 Torr pressure, at room temperature. The solid line shows the fit of the combined signals $(\mathcal{V}_U+\mathcal{V}_T)$. The dashed line shows the expected profile for $\mathcal{V}_U(y)$, based on jellium calculations for pure Cu ($r_s=2.67a_0$).

4. Surface scanning error

A surface scanning error signal, $\mathcal{V}_Y(\omega t)$ arises because the sample also translates laterally under the probe. If the work function of the sample surface is nonuniform (the patch effect), a spurious signal is generated because the probe periodically scans over a surface potential gradient. By moving the probe across the sample surface in the direction of translation under strain, y, a surface potential profile may be measured, reflected in a curve $V_{B0}(y)$. Then $\mathcal{V}_Y(\omega t)$ is given by

$$\mathcal{V}_Y(\omega t)=\frac{\partial V_{B0}}{\partial y}\frac{b'(\omega t)}{G(0)}\ , \tag{16}$$

where $b'(\omega t)$ is the periodic y-directed lateral motion of the sample relative to the probe. *Most earlier experimenters did not consider this problem at all, yet we found it to be the largest source of error, often more than 50% of the total measured signal.* Note the formal similarity between $\mathcal{V}_X$ and $\mathcal{V}_Y$ in Eqs. (16) and (17). We refer to these two signals collectively as the geometry error.

5. External couplings

Although steps were taken to minimize coupling of external ω signals from the electrical straining system and other external circuits, some may find their way into the measurement circuit. However, such signals have no connection with the spatial strain profile generated by bending the cantilevered bar, and may be thus distinguished as an overall offset $\mathcal{V}_{\text{offset}}(\omega t)$ in the spatial profile of $\mathcal{V}_{\text{total}}$, once it is corrected for $\mathcal{V}_X$ and $\mathcal{V}_Y$.

6. Thermal error

Strain also changes the temperature of the sample, analogously to the adiabatic compression of a gas. If different conductors are present in the measurement circuit, this generates thermoelectric emf's, although these may be shown to be generally negligible. However, the preexisting contact potential will also change due to the temperature dependence of the work function of the sample. Although a potentially large source of error, this was not considered by any of the earlier experimenters. This thermal error signal is given by

$$\mathcal{V}_T(y,\omega t)=\frac{1}{e}\frac{\partial W}{\partial T}T(y,\omega t)\ , \tag{17}$$

where $\partial W/\partial T$ is the temperature derivative of the sample's work function, and $T(y,\omega t)$ is the strain-induced temperature variation in the sample. Given the measured strain, $T(y,\omega t)$ may be determined from the solutions of the equations for thermal conduction in a strained body (Ref. 47, Sec. 32). The spatial profile of $T(y,\omega t)$ and hence of $\mathcal{V}_T(y,\omega t)$, is similar to the linear profile of the genuine signal, $\mathcal{V}_U$, making $\mathcal{V}_T(y,\omega t)$ difficult to distinguish (Fig. 5). However, if ω is small enough, there is a measurable phase shift, θ_T, with respect to the dilation, due to relaxation of the temperature variations. This phase shift, shown in Fig. 5 for $\omega/2\pi\approx 1$ Hz, may be used to separate $\mathcal{V}_T$.

7. Genuine signal

To summarize, we have identified four sources of spurious signal. Thus the total apparent strain-induced contact potential is given by

$$\mathcal{V}_{\text{total}}=\mathcal{V}_U+\mathcal{V}_X+\mathcal{V}_Y\mathcal{V}_{\text{offset}}+\mathcal{V}_T\ . \tag{18}$$

After all the quantities entering Eqs. (13)–(18) have been measured, $\mathcal{V}_X$ and $\mathcal{V}_Y$ may be subtracted from $\mathcal{V}_{\text{total}}$. The y profile of $\mathcal{V}_{\text{total}}-\mathcal{V}_X-\mathcal{V}_Y$ should then have an approximately linear profile due to $\mathcal{V}_U$ and $\mathcal{V}_T$, and an overall offset due to $\mathcal{V}_{\text{offset}}$. The latter may then be fitted and subtracted out, leaving $\mathcal{V}'=\mathcal{V}_{\text{total}}-\mathcal{V}_X-\mathcal{V}_Y-\mathcal{V}_{\text{offset}}$. Then $\partial W/\partial T$ and $\mathcal{V}_T$ are determined by

$$\frac{1}{e}\frac{\partial W}{\partial T}\frac{\mathcal{V}'(\omega t)|_{90^\circ}}{T(\omega t)|_{90^\circ}}\ , \tag{19}$$

$$\mathcal{V}_T(\omega t)=\frac{\mathcal{V}'(\omega t)|_{90^\circ}}{\sin\theta_T}\ , \tag{20}$$

where $|_{90^\circ}$ indicates the component of the preceding ac quantity that is in quadrature with the dilation (90° phase). Finally, subtracting $\mathcal{V}_T$ from $\mathcal{V}'$ leaves the genuine strain-induced contact potential $\mathcal{V}_U$. The strain derivative of the sample work function, $\partial W/\partial u$, is then determined from $\mathcal{V}_U$ and the measured dilation u by Eq. (11).

C. Apparatus

In essence, the apparatus in Fig. 3 measures the *total apparent* periodic contact-potential variation, $\mathcal{V}_{\text{total}}(y,\omega t)$, as well as any preexisting dc contact potential $\mathcal{V}_0$, between an unstrained capacitive probe and a sample surface periodically strained at $\omega/2\pi\approx 1$ Hz. The 5-mm-diameter stainless steel probe is vibrated in the x direction, normal to the sample surface, at a much higher frequency $\omega_0/2\pi\approx 500$ Hz. The resulting ac current from the probe, at frequencies ω_0 and $\omega_0\pm\omega$, is converted to a bias voltage with dc and ω components, V_{B0} and $V_B(y,\omega t)$, respectively, which are fed back to the capacitor through the probe. The equivalent circuit for the vibrating capacitor is in fact as shown in Fig. 2. This synchronous feedback loop system, based around lock-in no. 1, automates the null method of measuring contact potentials outlined previously. Lock-in no. 2 extracts $V_B(y,\omega t)$, and a high accuracy dc voltmeter measures V_{B0}.

The cantilevered bar is 512 mm tall, 10 mm thick, 30 mm wide, and made of A6061 aluminum alloy. An arrangement using a pair of solenoids provides an ω periodic bending force to the top of the bar in the y direction. This scheme is very useful in reducing $\mathcal{V}_{\text{offset}}$ because the solenoids provide a force at twice the frequency of their driving voltage. Thus the frequency of the high level driving voltage is $\omega/2$, and any coupling to the measurement circuit is effectively ignored by lock-in no. 2, which detects at ω. Strain gauges attached to the face opposite that sensed by the probe enable the strain to be measured there and then calculated at any other point on the bar.

A set of translation stages enables movement of the probe to, from, and across the face of the bar. Apart from electronic instrumentation, the apparatus is housed in a high vacuum system operating at room temperature. A cold trapped (77 K) oil-diffusion pump achieves 10^{-7} Torr pressure in the experimental chamber.

The region sensed by the probe was coated with thick films of either copper or gold, 2000 and 4000 Å thick, respectively, produced by evaporation from molybdenum boat sources. Any crystallites formed were smaller than about 10 μm. The Cu and Au sources were of 99.99+% and 99.99% purity, respectively. The apparatus was not capable of *in situ* film deposition, requiring a return to air, 5 h for Cu and 10 h for Au, before final pump-down for measurements. Other than this, the films were not disturbed in any way. An oxide layer and other adsorbed species would certainly have formed on the Cu film during this exposure. While Au does not readily oxidize, physisorbed species such as water would be present on the surface. We note that a complete set of measurements requires at least several days, thus it would be difficult to maintain atomically clean surfaces even if prepared and kept in ultrahigh vacuum for this period. In any case, such contaminated surfaces allow a meaningful comparison with the Cu drift tube surface used by WF, which received similar treatment.

We note that to participate in the same strain as the substrate, the metal films must adhere well to it. Physical inspection of the films after experiments were completed verified that they had not detached themselves from the substrate during the prolonged application of strain. In support of this, we note that a film would detach itself from the substrate if its elastic deformation energy exceeded its adhesion energy to the substrate. Given that the elastic energy density is given by $Ku^2/2$, where K is the bulk modulus[47], we require that $\delta(Ku^2/2)<\varepsilon$, where δ is the film thickness and ε is its adhesion energy per unit area. For most metals $K\approx 10^{11}$ N/m^2, the thickest film had $\delta=4000$Å, while $u<10^{-4}$. This requires $\varepsilon>0.013$ meV/Å^2. Since van der Waals interactions would provide adhesion energies at least of order 1 meV/Å^2, it is expected that even such weak adhesion suffices for our conditions.

V. EXPERIMENTAL RESULTS

After an initial data set for Cu was completed, another was acquired while the experimental vacuum space was filled with helium gas at 1 Torr pressure. While He is an inert gas, the temperature transition initially claimed by LWF, near the boiling point of He, suggested that He might be directly responsible for the absence of the DMRT field in their experiment. Although our apparatus was not capable of cryogenic operation, we felt it was worthwhile investigating the effects of a large amount of adsorbed He gas on the strain-induced contact potential, hence the reason for the relatively large ambient pressure. In yet another experiment, after evacuating the He, the Cu was exposed to oxygen gas at an ambient pressure of 3 Torr for 1 h, after which the O_2 gas was evacuated and the pressure returned to 10^{-7} Torr. In contrast to the He experiment, this is expected to significantly alter the surface chemistry. Measurements on Au were conducted at 10^{-7} Torr.

Unless otherwise noted, the uncertainties we quote in our results correspond to one standard deviation. These are the accumulation of random noise errors in all measurements, and calibration errors in instruments. We note that under the fixed conditions of each data set, repeated measurements made at the same position on the bar, two to three days apart from Cu and up to six days apart for Au, were reproducible within statistical error.

Figure 6 shows a typical y profile of $\mathcal{V}_{\text{total}}$ for Cu, while Fig. 7 shows the two geometry errors, $\mathcal{V}_X$ and $\mathcal{V}_Y$. Note the large deviation from a straight line in $\mathcal{V}_{\text{total}}$, mirrored by $\mathcal{V}_Y$. After subtracting these two errors from Fig. 6, we recover Fig. 8, showing an approximately straight-line profile for $\mathcal{V}_{\text{total}}-\mathcal{V}_X-\mathcal{V}_Y$, in accordance with that expected if this remaining signal is due to $\mathcal{V}_U+\mathcal{V}_T$. Note that there is no significant offset in the profile, revealing that the $\mathcal{V}_{\text{offset}}$ error is quite negligible. For comparison, Fig. 8 also shows the expected $\mathcal{V}_U$ signal for pure jellium Cu (dashed line). Although not yet corrected for the thermal error $\mathcal{V}_T$, we have recovered a signal that is of the same sign and close in magnitude to that predicted by the jellium model.

As noted in Sec. IV B, any thermal error signal would reveal itself by its phase shift relative to the dilation, particularly near the edges of the bar (Fig. 5). Figure 8 also shows the phase of the data points. All 12 data points at the left and right extremes (excepting one fluctuation) are reproducibly above zero by a few degrees. For points closer to the center, the signal level decreases and consequently the statistical error in determining the phase increases rapidly; moreover, $\mathcal{V}_T$ only shows large phase shifts away from the center. Thus the most accurate determination of $\mathcal{V}_T$ comes from the data near the edges. The point estimates for $\partial W/\partial T$, determined from Eq. (20), were averaged to reduce statistical error; Table IV shows the results for all data sets. Note that the values for the Cu surfaces are in good agreement with those expected for an oxidized Cu surface since $\partial W/\partial T$ is expected to have roughly the same value as the Seebeck coefficient,[51] which is known[52] to be close to 1 mV/K for CuO and Cu_2O. The value obtained for Au is significantly lower, although a non-negligible temperature dependence may be expected due to weakly physisorbed dipoles on the surface.

By use of Eq. (18) and the value of $\partial W/\partial T$, $\mathcal{V}_T$ was calculated and then subtracted from Fig. 8, leaving $\mathcal{V}_U$.

TABLE IV. Estimates of the mean $\partial W/\partial T$ over the face of the bar, derived from the phase-separation procedure (see text), at room temperature and 10^{-7} Torr unless otherwise noted.

Sample surface	$\partial W/\partial T$ (meV/K)
Cu initial	1.27±0.41
Cu in He gas at 1 Torr	1.83±0.47
Cu after increased oxidation	1.17±0.59
Au	0.35±0.25

TABLE V. Summary of measurements of $\partial W/\partial u$ at room temperature and 10^{-7} Torr vacuum, unless otherwise noted, and comparison with theory. The third column gives the implied DMRT field and the last column gives the ratio of the resulting electric force to that of gravity for particles used in drift tube experiments.

Surface	$\partial W/\partial u$ (eV/unit strain)	DMRT field (μV/m)	Ratio of electrical to gravitational force
Cu (initial)	-0.20 ± 0.04	-0.044 ± 0.009	800 for e^- and e^+ 0.4 for p and $\bar{p}$
Cu (in He gas at 1 Torr)	-0.23 ± 0.04	-0.051 ± 0.009	900 0.5
Cu (increased oxidation)	-0.46 ± 0.04	-0.10 ± 0.009	1800 1
Au	0 ± 0.05	0 ± 0.018	≤ 330 ≤ 0.18
Jellium Cu ($r_s=2.67a_0$)	-0.39	-0.083	1500 0.8
DMRT for Cu	0.5–5	0.1–1	1800–18 000 1–10
Jellium Au ($r_s=3.01a_0$)	-0.45	-0.16	2900 1.6

About half of the signal in Fig. 8 is due to $\mathcal{V}_T$. The total of all the spurious signals constitutes 70–80 % of the total measured signal, $\mathcal{V}_{\text{total}}$, which highlights the dangers present in these experiments. The mean value of $\partial W/\partial u$ across the face of the bar was determined from the ratio of the fitted slope, $\partial \mathcal{V}_U/\partial y$, to that of the dilation, $\partial u/\partial y$. The results are shown in Table V, along with the implied DMRT field, and theoretical estimates for comparison. The solid line in Fig. 8 shows the fitted $(\mathcal{V}_U+\mathcal{V}_T)$ signal.

The initial result for Cu in Table V has the same sign but about half the magnitude predicted by the jellium model. In the presence of He gas, there was no significant change in $\partial W/\partial u$, as may be expected given the inertness of He. In contrast, after increased oxidation, the value doubled, bringing it closer to the jellium prediction.

The result for the Au surface is more interesting, being at least an order of magnitude smaller than that predicted by jellium. All of $\mathcal{V}_{\text{total}}$ appeared to be spurious, mostly due to $\mathcal{V}_Y$. The partially corrected data, $\mathcal{V}_{\text{total}}-\mathcal{V}_X-\mathcal{V}_Y$ are shown in Fig. 9, in which we note that there is no evidence of a linear profile, certainly none comparable to that expected for jellium Au (dashed line). Our initial concern was that the Au film might not be adhering sufficiently well to the substrate, and thus might not be subject to the applied strain. However, our inspection of the surface and our estimate of the required binding energy (Sec. IV C) indicates that this was very unlikely to be the case.

We note that the residual data for Au appear to have a negative offset and slight evidence of spatial wiggles that are correlated with $\mathcal{V}_Y$, as if in correcting for $\mathcal{V}_Y$ we had slightly overestimated it. We have searched thoroughly for such systematic errors and found none. Earlier diagnostic experiments on this same surface showed much larger signals but drifting towards zero, which made it difficult to determine whether these were spurious or due to $\mathcal{V}_U$. This drift settled down in about a week, after which the data set in Fig. 9 was acquired. Over a period of six days of repeated measurements, these data were quite reproducible, within the statistical scatter evident in Fig. 9. Despite the unusual features, we are reasonably confident that a significant $\mathcal{V}_U$ signal would manifest itself by its linear profile, as it did for the Cu surfaces.

VI. SUMMARY AND CONCLUSIONS

We believe that we have identified and properly corrected for all the spurious effects present in our measurement of the strain-induced contact potential. Our investigations have shown that previous workers had failed to account adequately for spurious effects, as the wide distribution of results in Table III would indicate. Perhaps the most convincing feature of our data is the spatially linear signal profile obtained, which accords with the spatially linear strain gradient profile applied. This clearly establishes the presence of a tangential electric field just outside the surface. The measurements were highly reproducible and had uncertainties of 10–20 %, reasonably low given the amount of necessary correction.

The values obtained for $\partial W/\partial u$ were of the same sign and within the limits set by the jellium model, suggesting that this model may be quite a reasonable one for the real contaminated metal surfaces studied and for the similar Cu drift tube surface used by WF. Although we compared our results with the jellium model, we emphasize that the validity of our results is independent of any model. For Cu, $\partial W/\partial u$ was close in magnitude and sign to

that predicted by this model for the pure metal. Thus the expected DMRT field is about an order of magnitude smaller and of opposite sign to the original DMRT prediction.

In contrast, the Au surface showed no measurable strain-induced contact potential, implying $\partial W/\partial u$ is much smaller than even the jellium prediction for the pure metal. We cannot ascertain whether this is characteristic of Au itself or due to its adsorbed contaminants. We note that $\partial W/\partial u = 0$ is predicted by the jellium calculations for a jellium surface with $r_s \approx 1.8 a_0$. We would not have expected this for Au which has $r_s = 3.01 a_0$. It is possible that the apparent absence of the DMRT field in the WF experiment was due to such an"accident." However, our nonzero results for Cu make it clear that this is not an "accident" that can be consistently counted on.

In closing, we remark that due to sensitivity to surface conditions it is difficult to be certain that the results obtained for one surface sample, however reproducible, would also pertain to another sample, such as a drift tube surface. Studies of atomically clean surfaces are not necessarily relevant to drift tube surfaces as they cannot be made or maintained atomically clean. A prudent addition to future drift tube designs would be some mechanism for applying a known, variable, longitudinal strain gradient, in the drift tube walls, i.e., in addition to the gravitational strain. Then the DMRT field for the actual drift tube surface could be varied and studied *in situ*.

ACKNOWLEDGMENTS

We are indebted to Alberto Cimmino, Joseph Hajnal, and Tony Klein for many useful discussions. We gratefully acknowledge the support of the Australian Research Grants Committee.

[1]A. J. Dessler, F. C. Michel, H. E. Rorschach, and G. T. Trammell, Phys. Rev. **168**, 737 (1968).
[2]T. W. Darling, F. Rossi, G. I. Opat, and G. F. Moorhead, Rev. Mod. Phys. **64**, 237 (1992).
[3]F. C. Witteborn and W. M. Fairbank, Phys. Rev. Lett. **19**, 1049 (1967).
[4]W. M. Fairbank, F. C. Witteborn, J. M. J. Madey, and J. M. Lockhart, in *Experimental Gravitation,* edited by B. Bertotti (Academic, New York, 1974), p. 310.
[5]J. R. Henderson and W. M. Fairbank, in *LT-17 Conference Proceedings,* edited by U. Eckern *et al.* (Elsevier, New York, 1984), p. 1359.
[6]T. Goldman and M. M. Nieto, Phys. Lett. **112B**, 437 (1982).
[7]N. Beverini, J. H. Billen, B. E. Bonner, L. Bracci, R. E. Brown, L. J. Campbell, D. A. Church, K. R. Crandall, D. J. Ernst, A. L. Ford, T. Goldman, D. B. Holtkamp, M. H. Holzscheiter, S. D. Howe, R. J. Hughes, M. V. Hynes, N. Jarmie, R. A. Kenefick, N. S. P. King, V. Lagomarsino, G. Manuzio, M. M. Nieto, A. Picklesimer, R. M. Thaler, G. Torelli, T. P. Wangler, M. Weiss, and F. C. Witteborn (unpublished).
[8]F. C. Witteborn, Ph.D. thesis, Stanford University, 1965.
[9]F. Rossi, Ph.D. thesis, University of Melbourne, Australia, 1991.
[10]F. Rossi, G. I. Opat, and A. Cimmino, Rev. Sci. Instrum. (to be published).
[11]F. C. Witteborn and W. M. Fairbank, Rev. Sci. Instrum. **48**, 1 (1977).
[12]N. W. Ashcroft and N. D. Mermin, *Solid State Physics* (Holt, Rinehart and Winston, New York, 1976), Chap. 18.
[13]R. N. Varney and L. H. Fisher, Am. J. Phys. **48**, 405 (1980).
[14]M. S. Rzchowski and J. R. Henderson, Phys. Rev. A **38**, 4622 (1988).
[15]G. I. Opat, G. F. Moorhead, and F. Rossi (unpublished).
[16]T. W. Darling, Ph.D. thesis, University of Melbourne, 1989.
[17]F. Rossi and G. I. Opat (unpublished).
[18]R. S. Hanni and J. M. Madey, Phys. Rev. B **17**, 1976 (1978).
[19]N. Cabrera and N. F. Mott, Rep. Prog. Phys. **12**, 163 (1949).
[20]T. A. Delchar Surf. Sci. **27**, 11 (1971).
[21]L. I. Schiff and M. V. Barnhill, Phys. Rev. **151**, 1067 (1966).
[22]C. Herring, Phys. Rev. **171**, 1361 (1968).
[23]L. I. Schiff, Phys. Rev. B **1**, 4649 (1970).
[24]J. M. Lockhart, F. C. Witteborn, and W. M. Fairbank, Phys. Rev. Lett. **38**, 1220 (1977).
[25]J. M. Lockhart, F. C. Witteborn, and W. M. Fairbank, Phys. Rev. Lett. **67**, 283 (1991).
[26]M. S. Rzchowski, K. W. Rigby, and W. M. Fairbank, Jpn. J. Appl. Phys. **26**, 651 (1987), Supplement 26-3.
[27]N. D. Lang and W. Kohn, Phys. Rev. B **3**, 1215 (1971).
[28]S. C. Hunter and F. R. N. Nabarro, Proc. R. Soc. London, Ser. A **220**, 542 (1953).
[29]N. D. Lang and W. Kohn, Phys. Rev. B **1**, 4555 (1970).
[30]N. D. Lang and W. Kohn, Phys. Rev. B **7**, 3541 (1973).
[31]N. D. Lang and W. Kohn, Phys. Rev. B **8**, 6010 (1973).
[32]J. R. Smith, J. G. Gay, and F. J. Arlinghaus, Phys. Rev. B **21**, 2201 (1980).
[33]V. Russier and J. P. Badiali, Phys. Rev. B **39**, 13 193 (1989).
[34]V. Heine and C. H. Hodges, J. Phys. C **5**, 225 (1972).
[35]H. B. Michaelson, J. Appl. Phys. **48**, 4729 (1977).
[36]V. L. Moruzzi, J. F. Janak, and A. R. Williams, *Calculated Electronic Properties of Metals* (Pergamon, New York, 1978).
[37]N. D. Lang, in *Theory of the Inhomogeneous Electron Gas,* edited by S. Lundqvist and N. H. March (Plenum, New York, 1983), p. 323.
[38]J. P. Perdew and Y. Wang, Phys. Rev. B **38**, 12 228 (1988).
[39]W. Thomson (Lord Kelvin), Philos. Mag. **66**, 82 (1898).
[40]J. Hölzl and F. K. Schulte, in *Solid Surface Physics,* edited by G. Höhler, Springer Tracts in Modern Physics Vol. 85 (Springer-Verlag, Berlin, 1979), p. 1.
[41]P. P. Craig, Phys. Rev. Lett. **22**, 700 (1969).
[42]S. H. French and J. W. Beams, Phys. Rev. B **1**, 3300 (1970).
[43]J. C. Schumacher, W. E. Spicer, and W. A. Tiller (unpublished).
[44]C. R. Brown, J. B. Brown, E. Enga, and M. R. Halse, J. Phys. D **4**, 298 (1971).
[45]K. H. Leners, R. J. Kearney, and M. J. Dresser, Phys. Rev. B **6**, 2943 (1972).
[46]R. Chow and W. A. Tiller, J. Appl. Phys. **55**, 1339 (1984).
[47]L. D. Landau and E. M. Lifshitz, *Theory of Elasticity,* 2nd ed. (Pergamon, Oxford, 1970).
[48]R. J. D'Arcy and N. A. Surplice, J. Phys. D **3**, 482 (1970).

[49]B. Ritty, F. Wachtel, R. Manquenouille, F. Ott, and J. B. Donnet, J. Phys. E **15**, 310 (1982).
[50]F. Rossi (unpublished).
[51]C. Herring and M. H. Nichols, Rev. Mod. Phys. **21**, 185 (1949).
[52]*International Critical Tables of Numerical Data, Physics, Chemistry and Technology,* 1st ed., edited by E. W. Washburn (McGraw-Hill, New York, 1929), Vol. 6.
[53]J. W. Beams, Phys. Rev. Lett. **21**, 1093 (1968).
[54]E. W. Guptill, Can. J. Phys. **49**, 3150 (1971).
[55]E. Enga, Can. J. Phys. **52**, 708 (1974).
[56]R. I. Mints, V. P. Melekhin, and M. B. Partenskii, Fiz. Tverd. Tela (Leningrad) **16**, 3584 (1974) [Sov. Phys.—Solid State **16**, 2330 (1975)].